10   Phase Transitions, New Materials and Superconducting Photon Detectors

M. Reibelt, R. Dell'Amore, H. Bartolf, S. Siegrist (since October 2005), A. Engel and A. Schilling

in collaboration with: Paul Scherrer Institute (Ch. Rüegg, J. Mesot, M. Medarde, K. Pomjakushina, K. Conder), University of Bern (K. Krämer), Bhaba Atomic Research Center (G. Ravikumar), Forschungszentrum Karlsruhe (Th. Wolf, H. Küpfer), Universität Karlsruhe (K. Il'in), ETH Zürich (J. Karpinksi), Deutsches Zentrum für Luft- und Raumfahrt (H.-W. Hübers), CSEM Neuenburg, FIRST Lab ETH Zürich.

Last year we have started our activities at the FIRST Center for Micro- and Nanoscience at the ETH Zürich where we are exploring lift-off techniques as an alternative to electron-beam lithography for producing superconducting thin-film photon detectors (H. Bartolf and A. Engel). Within another new project supported by the NCCR MaNEP (Materials with Novel Electronic Properties) we have also started to synthesize and to study certain nickel oxides with the aim to explain some of their peculiar electronic properties (S. Siegrist). Details in the magnetic phase diagrams of the type-II superconductors V_3Si and $NbSe_2$ have been studied using a differential calorimeter (M. Reibelt), and a novel technique to detect possible resonance phenomena in $TlCuCl_3$ has been significantly improved and successfully tested on a quartz resonator (R. Dell'Amore).

10.1   Physics of superconducting thin-film nanostructures and possible applications as fast single-photon detectors

We investigate the properties of thin film superconductors, which we further structure into narrow bridges or meander lines with typical dimensions less than 10 nm thick and about 100 nm wide. The meander lines are of particular interest. It has been shown (1) that such structures, suitably operated, can be utilized as very fast and sensitive single-photon counters in the visible and near-infrared spectral range. Recently, such superconducting single-photon detectors have attracted increasing interest from such diverse fields as astronomy, spectroscopy or quantum cryptography.

In last year's annual report we have already discussed the principal detection mechanism for single photons in these nanostructured devices. There, we also introduced our refined detection model (2) that gives a much more consistent account of the experimental data. It follows from the detection mechanism that the cross-section of the strip line needs to be comparable in size to the cross-section of the quasi-particle cloud, hence the above mentioned dimensions in the 10 to 100 nm range. Otherwise, stable operation of the detector is hampered by inevitable noise superimposed on the bias current which needs to be closer to the equilibrium critical current of the strip the larger the cross-section is compared to the quasi-particle cloud. Further on, it is obviously also necessary for the strip line to be as homogeneous as possible along its entire length; chemically, morphologically and also geometrically, i.e. width and thickness have to be constant.

These requirements make great demands on lithography processes and device production technology. We have made great efforts to improve our situation in this respect. We have started, for example, to explore lift-off techniques as alternative means to obtain the required nanostructures. In Fig. 10.1 we show a cross-section of an already etched co-polymer
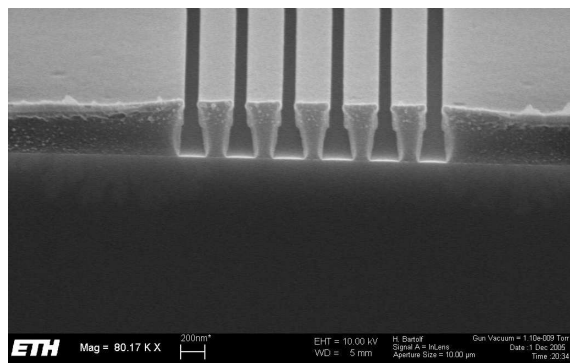
Figure 10.1: SEM-photo of the cross-section of a resist bi-layer. A set of parallel lines was written in the resist using e-beam lithography. The SEM examination was done after the etching process and before deposition of a metal film. The lift-off technique is based on a geometrical shadowing effect. After deposition the resist is removed using an appropriate solvent and the film deposited on top of the resist is washed away with it. The resulting line width would have been about 100 nm.

film before deposition and lift-off. First deposition tests with different metal films are promising and we are confident to be able to optimize the process parameters in order to obtain the necessary high-quality nanostructures. In Fig. 10.2 we show an example of one of the first successfully prepared meander structures. In this case a Ti-film was deposited onto a silicon substrate. The lines' width is about 200 nm and the film thickness is 5 nm. Also visible in this photo are 4 leads allowing for 4-point conductivity measurements. In further processing steps bonding pads overlapping with the leads will be deposited using photolithography.

A big advantage of this lift-off technique is the effortless adaptation to new superconducting materials other than the commonly used NbN. A shift to new materials seems to be necessary to increase the spectral range of these detectors. We have already shown in last year's report that with NbN the sensitivity will be limited to wavelengths below a few μm. The spectral sensitivity of NbN detectors is sufficient for applications using wavelengths near 1.3 and 1.5 μm, wavelengths commonly used in telecommunication. However, for astronomical applications for example, the limit should be pushed to wavelengths longer than 10 μm. This may be achieved with materials having lower T_c or much smaller strip cross-sections. At the other end of the spectral range, these detectors are interesting for x-ray spectroscopy due to their fast response and low jitter. Here, the absorption probability for x-ray photons needs to be increased; this implies the need for a superconductor with high Z-number.

Besides the efforts to increase the spectral range of these devices, it is also important to keep the noise, i.e. voltage pulses caused by effects other than the absorption of a photon, as low as possible. We have found indications that vortices could be a significant source of such dark counts (3). Other effects that could come into play are for example fluctuations in the quasi-particle density and thermal or even quantum phase-slips, depending on the dimensions of the strip line and the superconducting material used. These questions are also of fundamental interest and we have planned future experiments to shed light onto these issues.
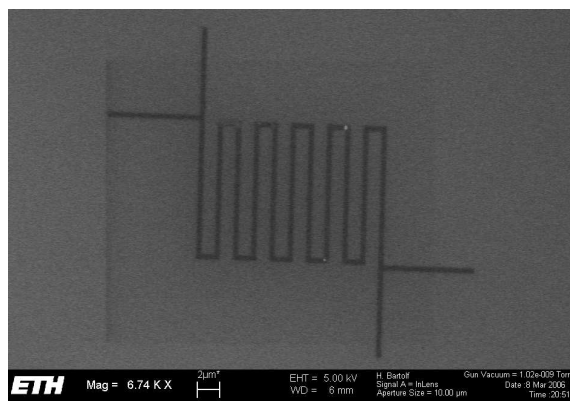

Figure 10.2: One of the first successfully prepared meander structures using the lift-off technique. In this SEM picture the meander appears as the dark structure. For test purposes a 5 nm thick Ti-film was deposited onto a silicon substrate. The linewidth in this case was approx. 200 nm.

In summary, we have developed a refined detection model for superconducting single-photon detectors. This new model gives a much more consistent description of experimental data. It also serves as the basis to describe fluctuation phenomena, which could be the origin of observed dark count rates. In this context we have found evidence that vortices also play a significant role. Within the report period we have also made substantial progress in lithography and device production.

[1] A. D. Semenov *et al.*, Physica C, **351**, (2001) 349.

[2] A. Semenov, *et al.*, submitted to Eur. Phys. J. B, **47**, (2005) 495.

[3] A. Engel, *et al.*, phys. stat. sol. (c), **2**, (2005) 1668.

10.2 Search for resonance phenomena in $TlCuCl_3$

In the last few years, quantum spin systems exhibiting magnetic-field-induced quantum phase transitions have attracted much attention (1; 2; 3). We have focused our work on $TlCuCl_3$, a 3D coupled spin ladder system, in which magnetic quasiparticles (magnons) are supposed to form a Bose-Einstein condensate above $\mu_0 H_c \approx$ 5.5 T at low temperatures (4). However, this BEC quantum phase transition requires the spin environment to be axially symmetric with respect to the applied magnetic field (5). ESR measurements, on the other hand, revealed a certain deviation from axial symmetry in $TlCuCl_3$ (6). To what extent this asymmetry precisely affects the quantum phase transition is not known.

Last year we have started to build an AC driven Wheatstone-like bridge set-up to detect resonance phenomena that can be expected if standing entropy waves form in a BEC. This work has been continued and significant improvements have been implemented. The bridge set-up is composed of two branches of identical coils and resistors, respectively. The same configuration, with the coils replaced by capacitors, can also be used to detect any kind of electrical or mechanical resonance. The drive signal is frequency modulated by the output signal of a lock-in amplifier. This signal is fed into the two branches of the bridge set-up. The voltage difference between the centers of
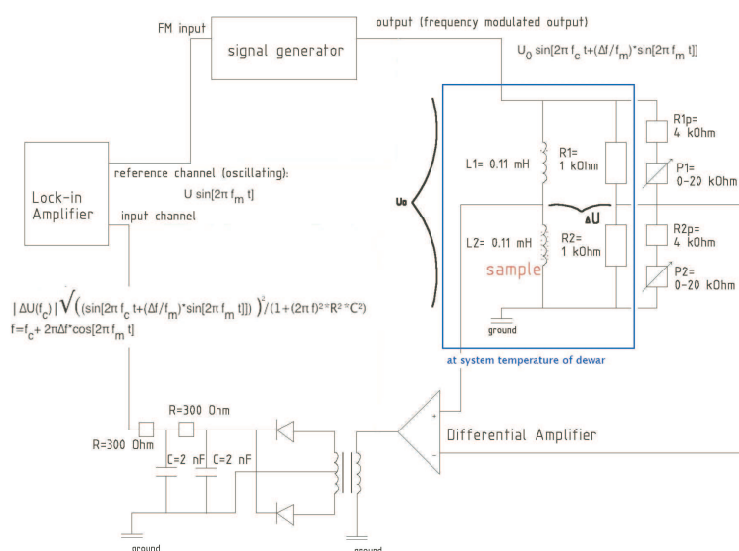

Figure 10.3: Bridge circuit to excite and detect collective modes in $TlCuCl_3$**. The carrier wave of varying frequency** $f_c =$**0.25-2 MHz is frequency modulated (**$f_m \ll f_c$**). The voltage difference** ΔU **across a balanced Wheatstone bridge composed of identical coils and resistors is amplified and rectified, low-pass filtered and analyzed with a lock-in amplifier. Absorption of energy by the sample in one of the coils should drive the bridge out of balance.**
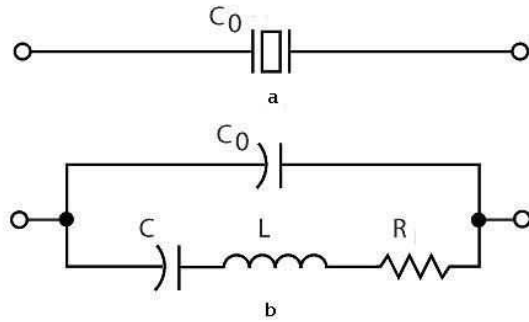
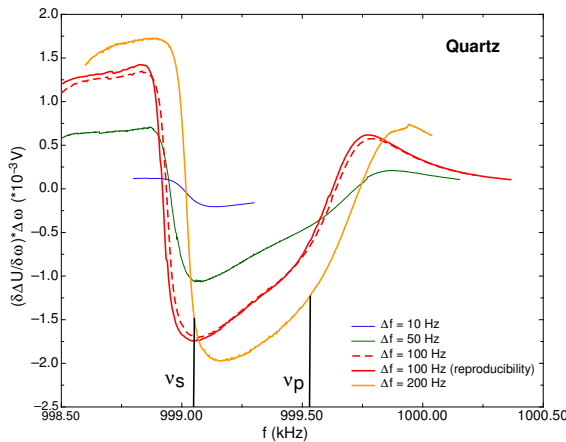**Figure 10.4: A quartz crystal in a shunt capacitance C_0 (a) and its equivalent circuit diagram (b).**

Figure 10.5: The resonances $\nu_{\rm s}$ and $\nu_{\rm p}$ detected on a quartz resonator.

the respective branches is detected differentially by low-capacitance probes. This voltage is then amplified, and the resulting signal is low-pass filtered to obtain a signal ΔU. This signal is measured with a lock-in amplifier, which now only varies with the modulation frequency f_m. By sweeping the carrier frequency f_c of the signal from 250 kHz to 4 MHz (self-resonance of the coil circuit), we can measure frequency dependent changes of the self inductance L or the capacitance C, respectively. The detected signal ΔU represents a measure for the derivative of the resonance curve with respect to frequency, whereas the peak-to-peak value scales with the standard-frequency deviation Δf (parameter of the signal generator) if this value is much smaller then the resonance linewidth $\Delta \nu$ ($\Delta f \ll \Delta \nu$).

As a first test we used a commercially available quartz crystal as a mechanical resonator, with a resonance frequency ν=1 MHz. The bridge set-up for this experiment consisted of two resistors on one branch and a resistor and a capacitance of similar impedance in this frequency range on the other branch. A piece of quartz in a shunt capacitance C_0 (Fig. 10.4a) can be regarded as a simple LCR resonating circuit (Fig. 10.4b), where the resistance R represents a measure for the losses, and C and L are equivalents for the elasticity of the quartz and mass of the vibrating crystal, respectively. Consequently, there are two close resonances $\nu_s =2\pi\frac{1}{\sqrt{LC}}$ and $\nu_p =2\pi\frac{1}{\sqrt{LC_0}}$, ($\nu_{\rm p} > \nu_{\rm s}$). Figure 10.5 shows the detected resonances using this technique.

Corresponding measurements on $\mathrm{TlCuCl_3}$ at T =2 K and $\mu_0 H$ =9 T have not yet revealed the resonances that can be expected in a possible BEC-state, however. A small but irreproducible background signal of unknown origin and the remaining electrical noise may still be too large to detect the expected small signals coming from the sample. Further changes on the set-up have been attempted to reduce the noise and to make a reasonable background subtraction possible. A step motor enables us now to move the sample in and out of the detection coil "in situ" in helium atmosphere. This allows us to perform an immediate background subtraction. Measurements with this new improved set-up are in progress.

[1] B. C. Watson et al., Phys. Rev. Lett. **86**, 5168 (2001).

[2] Ch. Rüegg et al., Nature **423**, 62 (2003).

[3] V. S. Zapf et al., Phys. Rev. Lett. **96**, 077204 (2006).

[4] T. Nikuni et al., Phys. Rev. Lett. **84**, 5868 (2000).

[5] I. Affleck et al., Phys. Rev. B **43**, 3215 (1991).

[6] V. N. Glazkov et al., Phys. Rev. B **69**, 184410 (2004)

10.3 Vortex phases in type-II superconductors

The physics of vortices in high-T_c superconductors has been a matter of active research because of its high relevance for the technical applications of these materials. In weakly pinned superconductors it should be possible to observe a transition of the vortex matter from a quasi-ordered Bragg glass (BG) to a disordered vortex solid or vortex glass (VG) phase (1). Pinning effects can lead to "superheating" or "supercooling" of the disordered phase (DP), and metastable phases of the vortex matter can be formed in the Bragg glass region. These metastable phases may hide first-order like phase transitions of an equilibrium state. In order to get access to the equilibrium state and to the respective phase diagram, one can use repeated quasi-static field cycling with a small amplitude (2) or a dynamic equilibration process involving a small AC field applied transverse to the DC field (vortex-shaking) (3; 4; 5; 6). We built a split-coil arrangement, which creates an AC magnetic field perpendicular to the main magnetic field, and we can also perform field-cycling loops to get access to the equilibrium state. First-order like magnetization steps below the onset of the peak effect (i.e., a sharp increase in the pinning force and critical-current density j_c as a function of field and/or temperature in conventional and high-T_c superconductors) have been recently observed in a single crystalline V_3Si sphere (7), and experiments on $NbSe_2$ also point in the same direction (8). However, no thermodynamic data on the different vortex phases and the respective phase transitions in these systems are available. Currently we are investigating the phase diagram of V_3Si and $NbSe_2$ with a differential-thermal analysis (DTA)-apparatus (9) that is particularly sensitive to phase transitions and allows us to conduct high-resolution specific-heat measurements.

V_3Si is in the clean limit, has a high Ginzburg-Landau parameter and a very small anisotropy. H. Küpfer from the Institut für Festkörperphysik, Forschungszentrum Karlsruhe (Germany) provided us with a spherical V_3Si sample on which first-order like features in the magnetization have been observed (1; 7). Since the orientation of the crystal with respect to the magnetic field is of importance, we let the sphere be oriented by G. Krauss from the Laboratorium für Kristallographie, ETH Zurich. A $NbSe_2$ single crystal was kindly provided to us by G. Ravikumar, Bhabha Atomic Research Centre, Mumbai (India). The $NbSe_2$ single crystal was a large, flat, thin disk ($m \approx 6.6$ mg), that we had to cut into pieces and stack them together using a small amount of *Apiezon* grease. This procedure resulted in a sample which has more surface roughness than a bulk object of equal mass. This circumstance and the lower T_c of $NbSe_2$ ($T_c \approx 7$ K) may make the investigation on $NbSe_2$ somewhat more difficult than on V_3Si.

In our first experiments on V_3Si we oriented the magnetic field away from the high symmetry axes of the crystal. The magnetic field was kept constant while we performed temperature sweeps. Figure 10.6 shows representative measurements on V_3Si for $\mu_0 H = 1$ T. The data exhibit many interesting features, but at the large scale to plot the data in Fig. 10.6 only the most pronounced ones can be seen. Besides the large discontinuity at T_c, the data show a
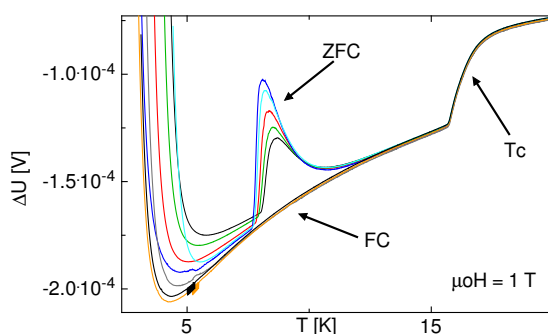
Figure 10.6: **Temperature sweep DTA-measurements on V_3Si at $\mu_0 H = 1$ T with different magnetic histories. From ΔU one can calculate the temperature difference between the two thermometers, and, in principle, the specific heat of the sample.**

strong self-heating effect around $T = 9$ K, which is history dependent and occurs only for zero-field cooling (ZFC), but not for a field-cooling (FC) history. This and other even more interesting features are currently under investigation. We are studying the influence of several parameters: The magnetic field H, the orientation of the symmetry axis (101) of the V_3Si sphere relative to the magnetic field, the temperature-sweep velocity, the strength of the magnetic AC-shaking field and its frequency, and the history dependence which results, for example, from the difference between zero-field cooling and field-cooling procedures.

[1] H. Küpfer, G. Ravikumar et al., Phys. Rev. B **70**, 144509 (2004).

[2] G. Ravikumar, V. C. Sahin et al., Phys. Rev. B **63**, 24505 (2001).

[3] M. Willemin et al., Phys. Rev. B **58**, R5940 (1998).

[4] M. Willemin et al., Phys. Rev. Lett. **81**, 4236 (1998).

[5] N. Avraham et al., Nature (London) **411**, 451 (2001).

[6] E. H. Brandt and G. P. Mikitik, Phys. Rev. Lett. **89**, 027002 (2002).

[7] G. Ravikumar and H. Küpfer, Phys. Rev. B **72**, 144530 (2005).

[8] S. S. Banerjee, N. G. Patil et al., preprint.

[9] A. Schilling and O. Jeandupeux, Phys. Rev. B **52**, 9714 (1995).

10.4   Synthesis and characterization of LaBaNiO$_{4-\delta}$

The compound LaBaNiO$_{4-\delta}$ is a structural analogue to LaSrNiO$_4$, and in particular to the well-known cuprate La$_2$CuO$_4$. While LaSrNiO$_4$ is known to be metallic (1), LaBaNiO$_{4-\delta}$ (at first sight an electronic analogue to LaSrNiO$_4$) is insulating or at least semiconducting (2). To clarify this issue we have prepared polycrystalline samples of LaBaNiO$_{4-\delta}$, and characterized them by X-ray diffraction, neutron diffraction, chemical analysis, resistivity, magnetic-susceptibility, and specific-heat measurements.

The neutron-diffraction data as well as a chemical analysis indicate that the LaBaNiO$_{4-\delta}$ samples are oxygen deficient ($\delta = 0.15$), which might also explain the observed superstructure (here interpreted as an oxygen-vacancy ordering), as well as the poor electrical conductivity as compared to LaSrNiO$_4$ (since also the planar oxygen atoms seem to be affected). We are therefore planning to try to ensure a full oxygenation of the LaBaNiO$_{4-\delta}$ samples by applying approriate oxygen-annealing techniques, and to repeat the various analysis experiments.

[1] R. J. Cava et al., Phys. Rev. B **43**, 1229 (1991).

[2] G. Demazeau et al., Mat. Res. Bull. **17**, 37 (1982).